Numerical modelling for rotational moulding with non-isothermal heating

K. K. Lim, A. Ianakiev, J. B. Hull

In the rotational moulding process, the internal air temperature has been widely recognised as a tool to predict an optimum cycle time. This paper presents a new numerical approach to predict the internal air temperature in a two-dimensional (2-D) static model without requiring the consideration of the tumbling motion of polymer powder. The initial non-isothermal heating of the static model is actually formed by two changeable plastic beds (stagnant and mixing beds), which represent the actual stagnant and mixing pools inside a rotating mould respectively. In the numerical approach, the lumped-parameter system and coincident node technique are proposed to incorporate with the Galerkin Finite Element Method in order to account for the complex thermal interaction of the internal air. It helps to overcome the difficulty of multidimensional static models in predicting an accurate internal air temperature during the heating stage of rotationally powdery plastic. Importantly, the predicted temperature profiles of the internal air, oven times for different part thicknesses and process conditions accord with the available experimental results. PRC/2029

Keywords: Rotational moulding (rotomoulding), Heat transfer, Finite element method (FEM), Lumped-parameter system, Coincident node technique, Deposition, Mixing pool, Stagnant pool, Mixing bed, Stagnant bed, Static bed model

 K. K. Lim (for correspondence E-mail, kok-khoon.lim@ntu.ac.uk), A. Ianakiev (E-mail, anton.ianakiev@ntu.ac.uk), and J. B. Hull (E-mail, barry.hull@ntu.ac.uk) are in the Division of Mechanical & Manufacturing Engineering, School of Computing and Technology, The Nottingham Trent University, Burton Street, Nottingham NG1 4BU, UK. Manuscript received 15 May 2003, accepted in final form 8 January 2004).

INTRODUCTION

Rotational moulding, also known as rotocasting or rotomoulding, is a method for producing hollow plastic articles. The final articles, such as water tanks and kayaks, are stress-free and environmentally friendly, with no-weld lines. Loading, heating, cooling and unloading are the four principal stages in the process as depicted in Fig. 1. At the loading station, an empty mould is filled with a pre-measured plastic powder with a typical particle size distribution[1] of –30 mesh (500 μm) to +200 mesh (70 μm). Then, the closed mould is heated in an oven whilst subjected to bi-axial motion. The speed of rotation is relatively low at 5–20 rpm. The heating process is accomplished by directly heating up the mould and the powder contained therein at an oven set-point temperature of about

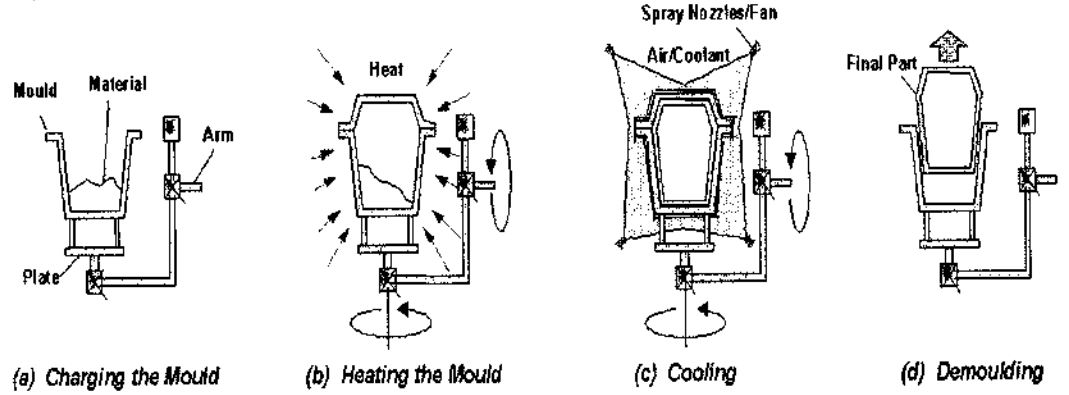

1 Principal stages of rotational moulding process (from Queen's University of Belfast website with permission from R. J. Crawford)

200–500°C. The plastic tumbles, softens and coats on the inner surface of the rotating mould at its 'tacky' temperatures. Eventually, a homogeneous liquid layer of polymer is formed. The molten product is then cooled until it has enough strength to retain the new mould shape (50–80°C). The mould is taken from the cooling bay and the rigid part is removed to end the rotomoulding cycle.

Trial-and-error methods and the measurement of the internal air and/or the external mould surface temperature are the common techniques used to determine heating and cooling cycles. Therefore, it would be cost effective and beneficial to develop numerical models to simulate, understand and improve the process. Roa and Throne[9] presented extensive experimental and theoretical studies on the factors that influence the process conditions of rotational moulding. They proposed a complicated model describing the heat transfer to the powder. Later, Gogos and Olson[3,4] introduced another new theoretical model in which well-mixed powder was assumed, and a one-dimensional (1-D) numerical approach was also presented to identify the key dimensionless groups affecting the process cycle times.

A series of experimental studies and improvements on numerical modelling have recently been done by workers at the Queen's University of Belfast.[2,10–13] Nugent[2] used a process controller, ROTOLOG, to record the real-time temperature profiles of the internal air and the oven. The approach helped to explore the plastic behaviour inside a closed mould and to calibrate numerical models. In addition, Nugent[2] also developed a rotomoulding simulation program to examine the bi-axial motion of a hollow mould containing a powder mass with a 1-D superimposed heat transfer mode. Later, Sun *et al.*[12] studied the efficiencies of 1-D internal heating and cooling effects with the ROHEAT program to improve the rotomoulding cycle time. The program, however, does not allow the effect of internal air to be explored. Furthermore, the ROHEAT program does not consider the impotency of the heat transfer between the inner mould surface and internal air at the initial stage of the rotomoulding process.[10] Improvements were made in the Liang *et al.*[10,11] 1-D model to enable a better prediction of the internal air temperature profile. In the model, the powder was initially assumed to be lying at the bottom of the mould and it would then be in static contact with all parts of the inner surface of the mould at the plastic melting temperature.

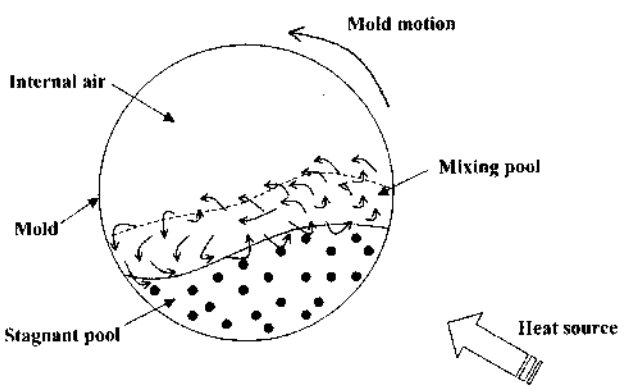

2 Axial motion of powder pools in rotating mould

According to Wright and Crawford,[19] the distribution of plastic is controlled by two main factors – kinematics of the mould and heat transfer to the plastic. After some improvements and substantial simplifications (i.e. isothermal melting temperature and fluidisation of the mixing pool), Wright and Crawford from Queen's University of Belfast have eventually developed a combined thermal and kinematic model for the rotational moulding process.[19] In brief, the kinematic model is used for predicting polymer distribution in the rotational moulding process. On the other hand, the thermal model for transient heat transfer was developed from the energy equation in which the continuous consumption of heating powder mass was imposed.

For multidimensional models, predicting the temperature of the internal air is still not possible. Wang[13] applied the Alternating Direction Implicit (ADI) method with a moving boundary to trace the plastic growth in a 2-D static model. The internal air temperature, however, is deviated substantially from the experimental result. The deviation was due to the fact that the internal air was heated through the plastic layer instead of through the mould at the beginning of the rotomoulding simulation; this assumption does not reflect the real situation in rotational moulding. In Gogos and Olson,[5–7] the growing plastic layer was tracked using the Arbitrary Lagrangian Eulerian technique at a distinct melting temperature. Owing to the assumption of well-mixed powder, unfortunately, the approach will have to neglect initially the thermal capacitance of the internal air compared to the thermal capacitance of the powder mass inside the revolving mould.

EXPERIMENTAL

Description of present approach: a two-dimensional static heating model

During the earliest stage of the rotational moulding process, a slowly rotating mould has its internal tumbling powder segregated into a stagnant pool and a mixing pool as shown in Fig. 2.[2] The figure also illustrates that only the lower surface of the stagnant pool is in perfect contact with the inner mould while leaving the upper mixing pool's surface exposed to the internal air. In view of this, the initial domain of the present static model is further being categorised into a stagnant/perfect-contact bed and a mixing/poor-contact bed (Fig. 3). These beds represent the stagnant and mixing pools, respectively. They behave like a solid body sticking to the inner mould wall throughout the entire cycle; the powder is assumed to be trapped inside

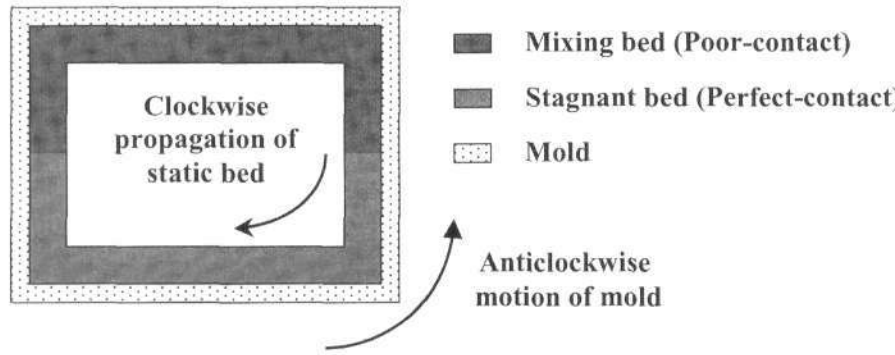

3 The geometrical domain of powder beds

the beds. Thus, no powder mixing is being considered. In fact, the mixing bed is formed by abutting its outermost interface with coincident nodes.[15] In addition, there is no consideration of radiation processes in the present thermal model. This is due to the early studies by Wright and Crawford which showed that these made only a very minor contribution to energy transfer.[19]

During the simulation, the plastic beds in Fig. 3 are continuously changing their positions representing the movement of the powder pool inside the rotating mould. Along with the 'dislocation', the elements of the plastic domains are gradually altering their position from stagnant (perfect-contact) to mixing (poor-contact) and *vice versa*. This is to ensure the plastic domains located against the inner mould surfaces vary with time. Whilst undergoing this cyclic dislocation, the plastic beds revisit and reprise on the initial co-ordinates of the model in order to circumvent the need to find new contact surfaces and re-computing the Jacobian matrices[17] in the finite element technique. When part of the predetermined bed achieves its tacky temperature, the mixing bed will gradually stick to the mould wall. This will be accompanied by the decreasing exposed surface of the inner mould to the internal air. Eventually, a completed stagnant bed is formed. Owing to the lack of technical descriptions for the process of heating tumbling powder, the actual re-contacted surfaces and residence time of the dislocation beds, and the friction/shear layer between the 'moving' mould surface and plastic surface against it have been ignored.

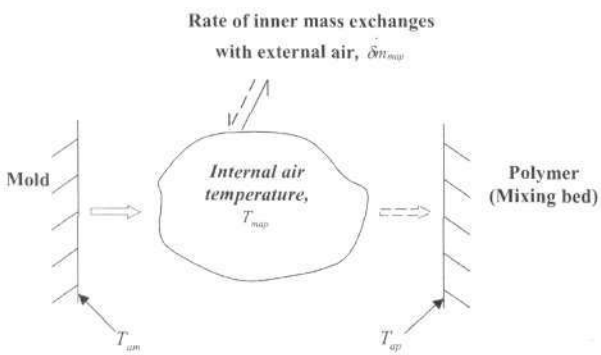

4 Mould–air–polymer thermal interaction for internal air (mould → internal air; T_{map} → polymer)

In practice, a mean value of the internal air temperature is taken to determine the cycle time, hence, the lumped-parameter approach[16] is employed to predict the temperature. With the lumped system, the energy balance of internal air temperatures owns to the 'mould–air–polymer' interaction (e.g. T_{map}) and 'mould–polymer–air' interaction (e.g. T_{mpa}) are treated separately, as illustrated in Figs. 4 and 5. The 'overall' internal air temperature inside the mould is then obtained via the thermodynamic equilibrium of the temperatures described by Equation (4), which will be discussed below. To simplify the mesh generation and minimise the mesh distortion, a square mould 315 mm × 315 mm is modelled which gives an equal total volume as the test case in steel trapezium mould – 330 mm × 330 mm at the top and 300 mm x 300 mm at the bottom.[2]

Governing equations for rotational moulding

The following governing equations have been used in the mathematical model of the rotational moulding process. The variable T represents temperature, whereas the subscripts m, p and a denote mould, plastic and internal air, respectively.

Energy equation of mould (Cartesian co-ordinate system)

Heat transfer through the mould is expressed by a transient heat conduction equation in which its thermal properties are assumed to be constant.

$$\rho_m c_m \frac{\partial T}{\partial t} = \left[\frac{\partial}{\partial x}\left(k_m \frac{\partial T}{\partial x} \right) + \frac{\partial}{\partial y}\left(k_m \frac{\partial T}{\partial y} \right) \right] \qquad (1)$$

Governing energy equation of polymer

The heat flow equation through the stagnant and mixing beds is represented by the non-linear transient conduction equation. The latent heat released or absorbed is directly incorporated into the effective heat capacity. Enichem RP246H polymer[10] is used but its properties are expressed in a discrete form instead (Table 1).

$$\rho_p c_p \frac{\partial T}{\partial t} = \left[\frac{\partial}{\partial x}\left(k_p \frac{\partial T}{\partial x} \right) + \frac{\partial}{\partial y}\left(k_p \frac{\partial T}{\partial y} \right) \right] \qquad (2)$$

Table 1 Enichem RP246H polymer properties (heating and cooling processes)9

Polymer properties	Notation	Temperature (K)			
		T < 363	363 ≤ T < 391	391 ≤ T < 407	407 ≤ T
Specific heat (J/kgK)	c_p	2377·9	3981·9	9973·4	2491·7
Thermal conductivity (W/mK)	k_p	0·1012	0·1012	0·1694	0·2774
Density for heating (kg/m³)	ρ_p	336·0000	343·2989	564·9044	860·3138
Density for cooling (kg/m³)	ρ_p	937·2254	908·9469	873·4154	860·4100

Governing energy equation of internal air (natural convection of ideal gas)

Equation (3) is used to deal with the energy balance of the internal air as shown schematically in Fig. 4. It illustrates that the internal air is directly heated by the mould. The equation also implies that the lumped-parameter analysis has neglected the internal resistance of the medium in comparison with the external resistance, mainly due to the poor thermal conductivity of air.

Thermal energy balance for the internal air =

Heat transfer of the external surrounding air with the internal air +

Heat transfer of the inner surface of the mould with the internal air +

Heat transfer of the inner surface of the plastic bed with the internal air

$$\left(m+\delta m_\gamma\right)c_{a,v}\frac{\partial T_\gamma}{\partial t}=$$

$$\delta m_\gamma\, c_{a,p}\left(T_{ex}-T_\gamma\right)+$$

$$\int_{S_{am}} h_{am}\left(\overline{T}_{am}-T_\gamma\right)\partial S_{am}+$$

$$\int_{S_{ap}} h_{ap}\left(\overline{T}_{am}-T_\gamma\right)\partial S_{ap} \qquad (3)$$

With the absence of the second term at the right-hand side of Equation (3), the direct mould–air interaction has been neglected. This means that only the direct 'mould–polymer–air' interaction of the internal air is accounted for, as depicted in Fig. 5. Here, T_{ex} is the external air temperature of the mould, and $\overline{T}_\gamma$ is the mean surface temperature of the surrounding medium to the internal air. The subscript γ can be either *map* or *mpa*. The subscripts *am* and *ap* describe the interfaces of mould–internal air and polymer–internal air, respectively. The parameter h is the heat transfer coefficient, m is the mass of air inside the mould, δm_γ is the net inner air mass exchanges with the external air for each time δt, and S is the heat transfer surface. Here, $C_{a,p}$ and $C_{a,v}$ are the specific heat of air at constant pressure and volume, respectively.[10]

The 'overall' thermodynamic equilibrium of the internal air is adopted for the above two different thermal interactions in Equation (3). The resultant temperature of the 'overall' internal air is:

$$T_a=(\theta+\varepsilon)T_{mpa}+(1-\theta-\varepsilon)T_{map} \qquad (4)$$

where:

$$\theta=(1-\varepsilon)\,fr \qquad (5)$$

and ε is the percentage of predominant T_{mpa} in the range $0 \le \varepsilon < 1$.

According to Equation 4, the thermal correlation between the Figs. 4 and 5 could be related to the fractional ratio (*fr*) of Equation (5). The function is presumed to have a relationship between the thermal stage of the mixing bed and its tacky temperature. In fact, the percentages of energy exchange among the mould, powder and internal air are ambiguous owing to the complexities of their thermal interactions inside the revolving mould. Thus, the experimental test cases from two different authors[2,11] are used to verify the predicted results and also the correlation of *fr* to the process.

Boundary condition 1: outer mould surface by external force air convection

A homogeneous oven temperature is assumed, and the type of heating/cooling method can be accounted for by using the external heat transfer coefficient (h_{ow}).

$$q=h_{ow}\left(T-T_{ow}\right) \qquad \text{on } \Gamma_{ow} \qquad (6)$$

where T_{ow} can be either the temperature of the external heating air (T_{ow}) or the cooling air (T_{oc}).

Boundary condition 2: mould-stagnant bed interface (perfect contact)

The bulk flow of the stagnant pool is relatively still, where heat conduction is a dominant factor. For the stagnant bed, therefore, a continuous heat flux is imposed to its mould-plastic interface (Γ_{mp}).

$$-k_m\left.\frac{\partial T}{\partial n}\right|_m=-k_p\left.\frac{\partial T}{\partial n}\right|_p \qquad \text{on } \Gamma_{mp} \qquad (7)$$

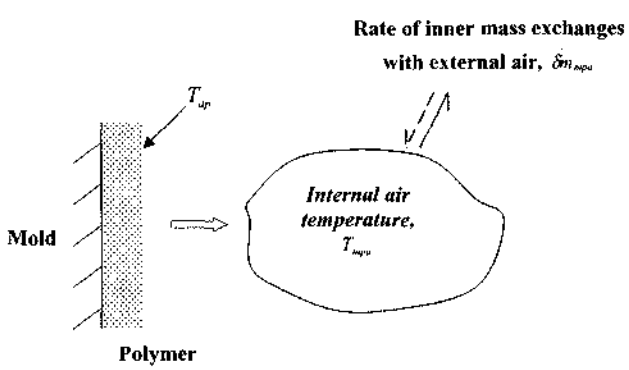

5 Mould–polymer–air thermal interaction for internal air (mould → polymer; T_{mpa} → internal air)

Boundary condition 3: mould–mixing bed interface (non-perfect contact)

The heat is likely transferred from the mould to the dynamic mixing pool via a convection process. As a result, the mixing bed is formed by abutting its mould–plastic interface (Γ_{mi}) with a layer of air gap using the coincident node technique[15] shown in Fig. 6. This brings about a new element conductivity matrix as:

$$\underline{K}^e_{int} = \int_{\Gamma^e_{int}} \left(h_{am} N_j \left(N_i - \frac{1}{2} N_g \right) \right) \partial \Gamma^e_{int} \qquad \text{on } \Gamma^e_{int} \quad (8)$$

where $i,j = 1, 2, \ldots, cn_f$.

Here, cn_f is the number of nodes on the mould–plastic interface boundary, and the subscript g is the number of the node coincident with i. The superscript e stands for an element. This integration is performed for the elements on both sides of the interface. As a result of this, the final element conductivity matrix ($\underline{K}^e$) becomes:

$$\underline{K}^e = \underline{K}^e + \underline{K}^e_{int} \quad (9)$$

The details of the Finite Element Method (FEM), however, are discussed below.

Boundary condition 4: inner plastic surface and internal air

The convective heat transfer for the interface between the inner plastic surface and internal air (Γ_{ap}) is described by:

$$q = h_{ap}(T - T_{mpa}) \qquad \text{on } \Gamma_{ap} \quad (10)$$

Numerical discretisation of the governing equations: Finite Element Method

The Galerkin weighted residual finite element method[17] is employed for partial differential equation (PDE) discretisation. In the Galerkin method, the weighted residual (W_i) is chosen equal to the shape function (N_i). The 8-noded serendipity element is used for the model. The variations of temperature throughout the element domain are approximated in terms of values T_j as follows:

$$T = \sum_{j=1}^{nd} N_j(x,y) T_j(t) \quad (11)$$

where nd is nodes per element.

A co-ordinate transformation is performed to transform the global co-ordinate to the local co-ordinate systems, which allows the global co-ordinates to be written in interpolation form as:

$$x = \sum_{j=1}^{nd} N_j(\xi,\eta) x_j \quad (12)$$

$$y = \sum_{j=1}^{nd} N_j(\xi,\eta) y_j \quad (13)$$

Here, the discretisation process of the governing energy equations comprises two parts – spatial discretisation and temporal discretisation. By performing the weighted residual integration over an element domain Ω^e, the governing Equations (1–3) are expressed as the following weak form of Equations (14–16):

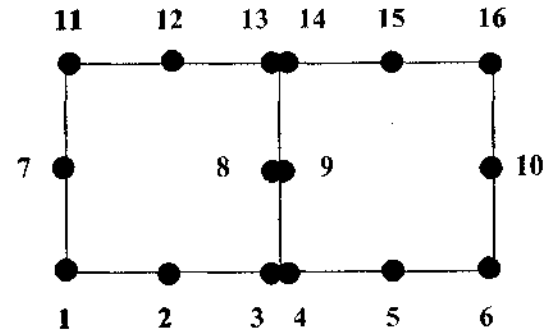

6 Co-incident node elements for air-gap formation within the interface of the mould and mixing bed

Spatial discretisation of the linear heat conduction equation for mould

$$\int_{\Omega^e} \rho_m c_m N_i N_j \partial \Omega^e \frac{\partial T_j}{\partial t} + \left\{ \int_{\Omega^e} k_m \nabla N_i \nabla N_j \partial \Omega^e + \int_{\Gamma^e} h_{ow} N_i N_j \partial \Gamma^e \right\} T_j = \int_{\Gamma^e} h_{ow} T_{ow} N_i \partial \Gamma^e \quad (14)$$

where $\partial \Omega^e = |J| \partial \xi \partial \eta$ and $\partial \Gamma^e = |J| \partial \xi$. The determinants $|J|$ and $|J_\Gamma|$ are the determinants of the Jacobian operator for 2-D and 1-D domains, respectively.[17]

Spatial discretisation of the non-linear heat conduction equation for polymer

After the discretisation, the energy Equation (2) of polymer becomes:

$$\int_{\Omega^e} \rho_p c_p N_i N_j \partial \Omega^e \frac{\partial T_j}{\partial t} + \left\{ \int_{\Omega^e} k_p \nabla N_i \nabla N_j \partial \Omega^e + \int_{\Gamma^e} h_{ap} N_i N_j \partial \Gamma^e \right\} T_j = \int_{\Gamma^e} h_{ap} T_{mpa} N_i \partial \Gamma^e \quad (15)$$

where the superscript n refers to the previous time step.

Spatial discretisation of the heat conduction equation for internal air

The explicit approach is requested for T_{imap} at each time step. In the meantime, therefore, another explicit approximation is also applied to the T_{mpa} of energy Equation (3) for minimising computational time. Indeed, no spatial discretisation is needed for the internal air model. This is because it is treated as a bulk node – a zero-dimensional model. This means the bulk node is arbitrarily located within the domain, and is characterised by a single temperature $T_\gamma(t)$. To standardise the mathematical expression, the equation is presented in the finite element form as follows:

$$N_j(m + \delta m) c_{a,\gamma} \frac{\partial T_{j,\gamma}}{\partial t} + \left(N_j \delta m c_{a,\gamma} + \int_{\Gamma^e_{am}} N_j h_{am} \partial \Gamma^e_{am} + \int_{\Gamma^e_{ap}} N_j h_{ap} \partial \Gamma^e_{ap} \right) T_{j,\gamma}$$

$$=\delta m c_{\alpha,p} T_{\alpha x} + \int_{\Gamma_{am}} h_{am} \bar{T}^{n}_{am} \partial\Gamma^{e}_{am} + \int_{\Gamma_{ap}} h_{ap} \bar{T}^{n}_{ap} \partial\Gamma^{e}_{ap} \quad (16)$$

The completed spatial discretisation of the energy Equations (14–16) can be presented in matrix form as follows:

$$\underline{C}^{e}(T^{*})T + \underline{K}^{e}(T^{*})T = \underline{F}^{e} \quad (17)$$

Here, T stands for $\frac{\partial T}{\partial t}$, whereas $\underline{C}^{e}(T^{*})$, $\underline{K}^{e}(T^{*})$ and $\underline{F}^{e}$ are mass matrix, stiffness matrix and forcing vector of an element respectively. The T^{*} term in Equation (17) can be expressed as:

$$T^{*} = \frac{1}{2}\left(T^{n} + T^{n-1}\right) \quad (18)$$

where the superscripts n and $n-1$ are referring to previous time steps.

Temporal discretisation of mould and polymer heat conduction equations

The unconditional stable Dupont II scheme[18] ($a = 1/4$) is chosen for solving the final global partially discretised energy Equations (14 and 15). Iteration is still carried out at each time step owing to the continuous change in contact surface and non-linearity of the polymer properties.

$$\left(\underline{C} + \frac{3}{4}\Delta t\underline{K}\right)T^{n+1} = \underline{C}T^{n} - \frac{1}{4}\Delta t\underline{K}T^{n-1} + \Delta t\underline{F} \quad (19)$$

The new predicted temperatures from Equation (19) are used to update the internal air temperature of the governing Equation (16) with the Crank-Nicolson method ($\theta = 1/2$).[17]

$$\left(\underline{C} + \frac{1}{2}\Delta t\underline{K}\right)T^{n+1} = \left(\underline{C} - \frac{1}{2}\Delta t\underline{K}\right)T^{n} + \frac{1}{2}\Delta t\left(\underline{F}^{n+1} + \underline{F}^{n}\right) \quad (20)$$

RESULTS AND DISCUSSION

To verify the basic finite element discretised energy equations of the present model, the output temperature profile of the external mould surface is compared with the available experimental result[2] as depicted in Fig. 7. The result shows that the present model gives a satisfactory prediction of the mould temperature profile during a 2·7 mm plastic part simulation. Therefore, the basic numerical codes have been confirmed.

From the modelling viewpoint of rotational moulding, the usefulness of a model should minimally be judged on its ability to predict the process times (heating time and cooling time) and to identify the six major stages of a completed rotational moulding cycle using the internal air temperature (Table 2). As stated in Table 2, each stage of the internal air temperature does describe the physical change of a polymer during the process. Here the satisfactory prediction in Fig. 8 has proved the basic feasibility of the present approach/model for the rotational moulding process. At stage 2 in Fig. 8, some deviation from the experimental temperature profile is observed. Perhaps this is because the present attempt only considers a single deposition of mixing bed between the outer interface of the bed and inner mould surface. Thus, the assumption has neglected the complex thermal interaction of internal air resulting from layer-by-layer deposition of plastic in practice. In addition, it also contributed to the no mixing assumption (i.e. pre-arranged polymeric static model). At stage 3, a better prediction of the internal air temperature is observed particularly when the temperature approaches 200°C (Fig. 8). This is because of the similarity of the physical stage between the actual plastic bed and numerical model.

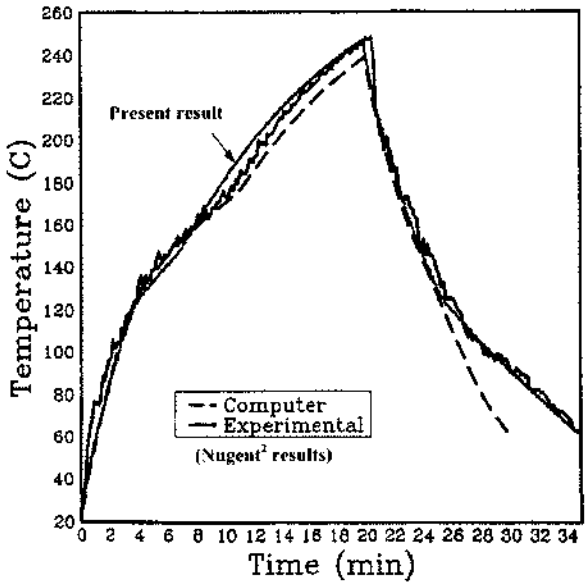

7 Comparison between experimental and predicted external wall temperatures (RP246H – 2·7 mm plastic part – steel mould – 300°C oven)

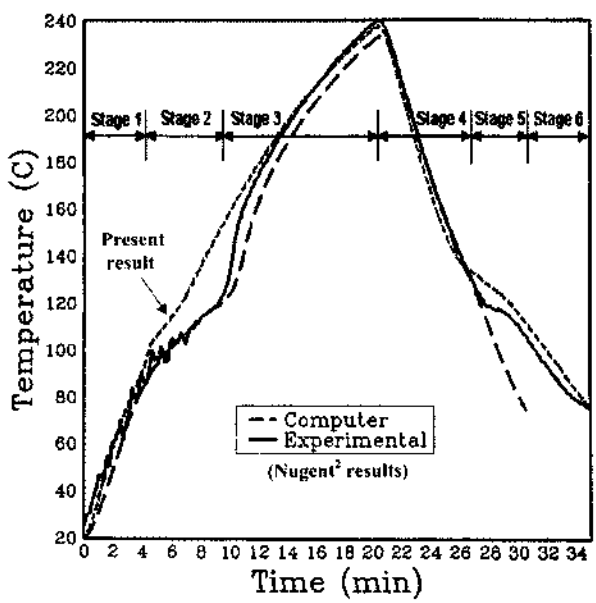

8 Comparison between experimental and predicted internal air temperatures (RP246H – 2·7 mm plastic part – steel mould – 300°C oven)

Table 2 Physical and numerical representation of plastic in rotational moulding process

Process	Internal air					
	Heating			Cooling		
Rotational moulding process	Stage 1	Stage 2	Stage 3	Stage 4	Stage 5	Stage 6
Physical stage of plastic	Free powder	Free powder and molten plastic	Melted plastic	Melted plastic	Molten and solid plastics	Solid plastic
Remarks of present model	Mixing and stagnant beds	Mixing and stagnant beds	Stagnant bed	Stagnant bed	Stagnant bed	Stagnant bed

Table 3 Heat transfer coefficients (h_{ov})

	Thin part	Medium part	Thick part	Remarks
Part Margin, δ_p (mm)	$0 < \delta_p \leq 5$	$5 < \delta_p \leq 9$	$9 < \delta_p \leq 12$	–
h_{ov} (W/m^{2}K)	17	16	15	Oven–mould interface (heating)

Table 3 shows how a set of h_{ov} is defined and required for a range of part thickness in the present model. The narrow margin of h_{ov} (15–17 W/m^{2}K) is selected after some careful comparisons between the predicted and experimental results of an empty mould surface shown in Fig. 9. This is to ensure that the chosen values do not disobey the external process condition of the actual experiment; either upper or lower limit of the mean h_{ov} is applied, the simulation still obeys the process state. As a result, the methodology of varying the mean h_{ov} will not imply any alteration of the moulding condition. On the other hand, the assigned range of thin, medium and thick parts in Table 3 are testified by the results in Fig. 14. The table also indicates the thicker the part the less the h_{ov} is needed. The requirement of the variation (h_{ov}) is employed for the following reasons:

(i) The main intention is to compensate the pre-arranged polymeric static bed of the present model since the onset of each simulation, which is not fully compliant with the physical heating condition of the rotational moulding. For instance, the mixing of tumbling powder is absent from this model.

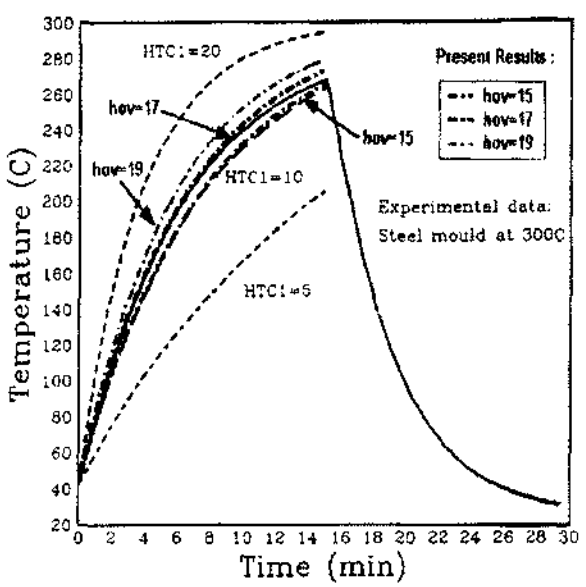

9 Predicted effects of external heat transfer coefficient on mould surface temperature[2] using empty steel mould at 300°C

(ii) In the authors' opinion, the locations at mould surface, where the heat transfer coefficients are measured, should be taken and biased towards the mould locations frequently retaining the powder. This is because the heat transfer towards the surface plays a relatively significant role in heating up and melting the powder. Of course the closer the mould surface to the external heat source, the higher the mean value of the measured heat transfer coefficient. Since the mixing rate of powder might vary with the compactibility of a mould, therefore, the measuring locations could also be varying with the amount of powder mass. In a less packing mould (little powder mass or thin part), for example, the 'overall' tumbling powder will expect to have more frequent contact with the enclosed hotter mould surface owing to a relatively fast mixing rate. From the perspective of the above interpretation, the mean h_{ov} of thin part could be slightly higher; therefore, it is allowed to be set at the highest margin of h_{ov} and vice-versa. As a result, the variations of h_{ov} in Table 3 can be treated as how frequently the overall powder spends against various hot spots of its inner mould surfaces (i.e. Fig. 2), owing to the different mixing intensity of the plastic powder inside a fixed volume of the mould. With this methodology, the fast, medium and slow mixing rates (with respect to fixed volume of mould) arise. They refer to the cases describing thin, medium and thick parts, respectively, and are categorised by the different averaged h_{ov} within a reasonable process margin.

(iii) The external heating coefficient (h_{ov}) was actually found to lie within a margin of 8–13 W/m^{2}K in the Nugent thesis.[2] Perhaps the dissimilarity between

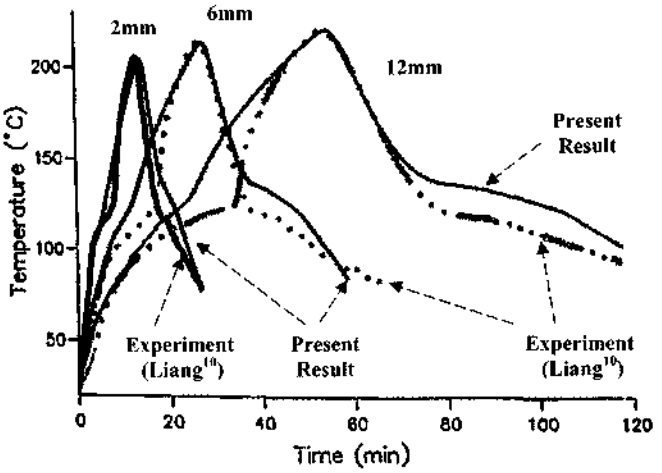

10 Comparisons between experimental and predicted internal air temperatures of 2, 6 and 12 mm part thicknesses

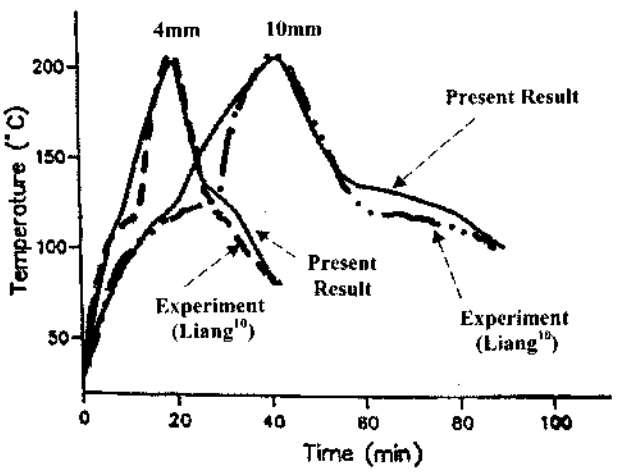

11 Comparisons between experimental and predicted internal air temperatures of 4 and 10 mm part thicknesses

the present and Nugent values for h_{ov} is contributed to by the difference in the approaches and some variations in the process conditions. It is indeed very difficult to measure h_{ov} without any bias in practice as the actual values of h_{ov} are highly dependent on where the thermocouples located on a mould facing the external source as sketched in Fig. 2. Furthermore, the arms of machine and mould carrier (spider) also act as a shield causing the variations in the mean h_{ov} in practice.

Based on the above three statements, therefore, it would be sensible to categorise the heating coefficient within a reasonable margin (i.e. Table 3) for different ranges of part thickness. The approach also aims to seek a marginal accuracy of the predicted outputs. Based on Figs. 7, 10 and 14, for example, the correlations between the heat transfer coefficients and the available experimental results are good when they are coupled with the present governing equations. Of course a single value of h_{ov} for any modelling is the most desirable in order not to be restricted by the thickness of part.

Figs. 10 and 11 show the comparisons between predicted and experimental[11] temperature profiles of the internal air across a range of part thickness. The essential data such as initial powder temperature, heating time, part thickness and mould dimension for the simulations are originally abstracted from Table 5–7 of Liang's thesis.[11] However, the uncertain external oven conditions are presumed similar to the Nugent experiment[2] with a similar mould dimension (as the sources for comparisons were taken from the same university – Queen's University, Belfast). Generally, the predictions are satisfied in particular at stage 1 of the rotomoulding cycle. It is considered a difficult, but the most important, stage to be modelled. This is because the success or failure of present/any rotomoulding model in predicting and symbolising the internal air temperature profile of the process is strongly dependent on how the thermal interaction of

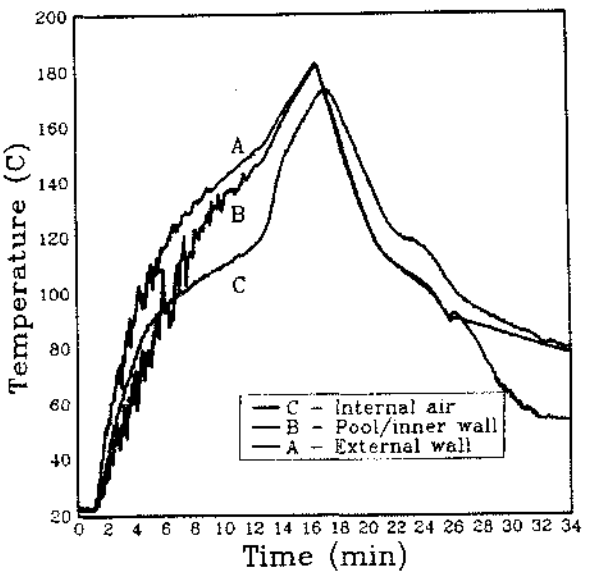

12 Sample of experimental temperature profiles during a rotational moulding cycle[2] (with the permission of Dr Nugent)

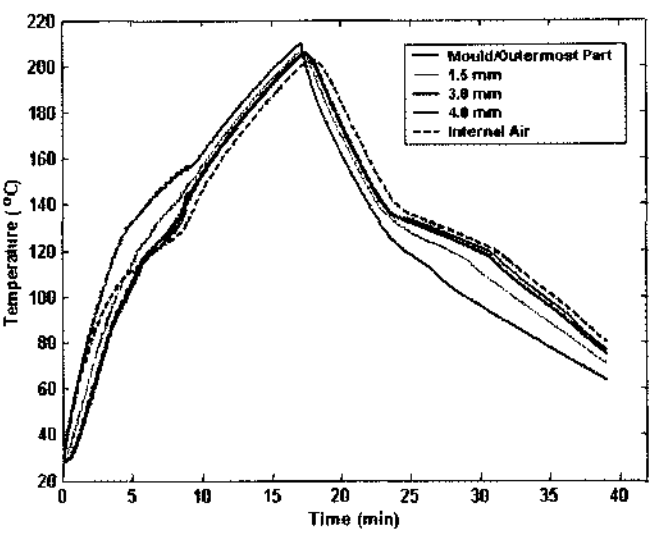

13 Predicted temperature profiles of the internal air and various points across a 4 mm part thickness

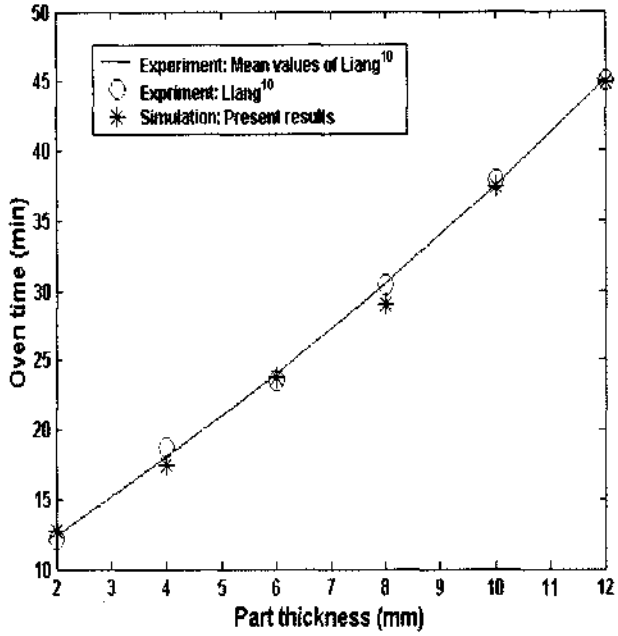

14 Predicted and experimental oven times to internal air temperatures of 200°C for a range of part wall thickness (RP246H – steel mould)

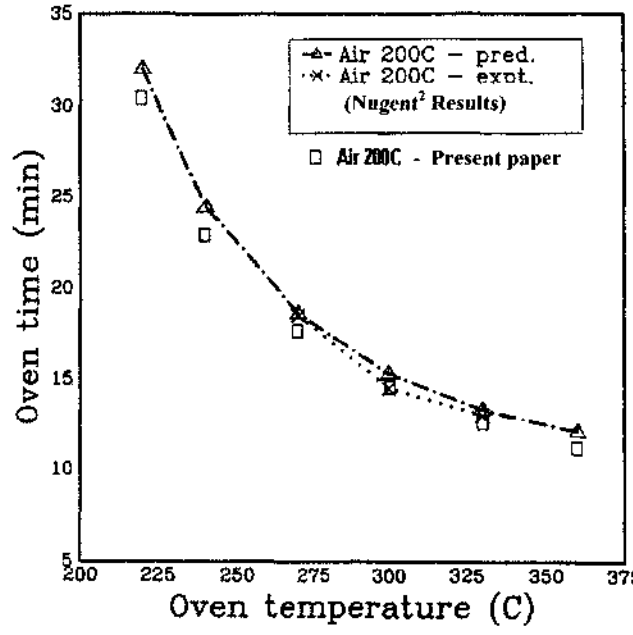

15 Predicted and experimental oven times to internal air temperatures of 200°C for a range of oven settings (RP246H – steel mould – 300°C oven)

bulk air is accounted for during stage 1. A 12 mm thick part in Fig. 10, for example, still shows a good predicted internal air temperature for the first 20 min of the rotomoulding cycle. This implies that the present static approach can handle the complex thermal interactions of the internal air with its surrounding media at stage 1 even without involving the modelling of changeable tumbling powder mass and its location inside the mould. A deviation is observed at stage 2 of the heating cycle and can be explained as discussed above. For the cooling cycle, Figs. 10 and 11 show that the predicted temperature profiles resemble, or are even closer to, the experimental plots using a single value of h_{ov}.

The caption to Fig. 12 shows the experimental profiles of mould, powder pool and internal air during a rotational moulding cycle. The figure shows that the temperature of the internal air is higher than the powder pool but lower than the mould during the earliest period of the process. This is because the internal air is directly heated by the mould rather than by the powder pool. The temperature of the powder pool only surpasses the internal air after some time the melting plateau previews. It is noteworthy that this phenomenon is observed in the present model (Fig. 13). During stage 1, however, the predicted profile of internal air temperature is found to be somewhat higher. This implies some improvements on the thermal interaction between the internal air and its surrounding media are still needed in order to bring the predicted air profile closer to the experimental phenomenon (i.e. inner air temperature is lower than mould but higher than powder pool). Finally, the comparisons on the effect of oven temperature on the heating/oven time have been shown in Fig. 15. The predicted results also correlate well with the available experimental results[2] for a range of oven settings.

CONCLUSIONS

The coincident node technique, conventionally used to treat a warpage formation, has shown its potential to be incorporated with the lumped-parameter system and finite element technique for predicting the internal air temperature during the powder heating of the rotational moulding process. The technique also proves its flexibility in handling problems with changeable contacted surfaces. With some simplified assumptions, the present methodology of modelling has managed to predict the temperature profile of internal air resembling the real-world result. A notable feature of the approach is that this static bed model is capable of producing a satisfactory result for the internal air temperature at stage 1 (vigorous powder mixing involved) without the consideration of powder movement and the change of powder mass. Thus, the technique has obviated the need to find an exact movement of powder pool during the thermal simulation of the powdery polymer. This makes the rotomoulding modelling much simpler. In addition, the approach also gives a good prediction of oven time over a range of oven temperatures and part thicknesses for at least up to 12 mm part thickness. The overall results indicate that the present difficulty in predicting a satisfactory internal air temperature profile in a multidimensional model has been overcome.

Further work will analyse phase change (solidification) in detail and simulations of warpage

phenomenon during the rotomoulding cooling process. Also, future studies and improvements, such as the 'layer-by-layer deposition' model and single value of h_{ov} are needed to give a better predicted temperature profile of the internal air for the entire rotomoulding cycle. In addition, a semi-implicit approach for solving the internal air equation is recommended, particularly for the warpage problem.

ACKNOWLEDGEMENTS

The authors would like to thank Prof. R. J. Crawford for granting permission to use the illustration from Queen's University of Belfast for the publication. We also thank Dr P. J. Nugent for his generosity in sharing his valuable experimental and numerical results for comparison. Thanks are also due to Mr M. Spencer and Rototek Ltd for sharing their views and first-hand experience, which have contributed to the progress of the research.

REFERENCES

1. R. J. CRAWFORD and J. L. THRONE: 'Rotational Molding Technology', 1st edn. Portland, William Andrew, 2001, 315.
2. P. J. NUGENT: PhD Thesis, Queen's University, Belfast, 1990.
3. L. G. OLSON, G. GOGOS, V. PASHAM and X. LIU: Numerical Modeling For Rotational Moulding of Thermoplastics, Proc. ASME Heat Transfer Division, 1997, **1**, 113–119.
4. G. GOGOS, L. G. OLSON, X. LIU and V. PASHAM: *Polym. Eng. Sci.*, 1998, **38**, 1387–1397.
5. L. G. OLSON, G. GOGOS, V. PASHAM and N. GEIGER: *Polym. Eng. Sci.*, 2000, **40**, 1758–1764.
6. L. G. OLSON, G. GOGOS and V. PASHAM: *Int. J. Num. Methods Heat Fluid Flow*, 1999, **9**, 515–542.
7. G. GOGOS, L. G. OLSON and X. LIU: *Polym. Eng. Sci.*, 1999, **39**, 617–629.
8. R. C. PROGELHOF, G. CELLIER and J. THRONE: Proc. ANTEC, SPE, 1982, 627–629.
9. M. A. RAO and J. L. THRONE: *Polym. Eng. Sci.*, 1972, **12**, 237–264.
10. LIANG XU and R. J. CRAWFORD: *Plastics, Rubber Composites Proc. Appl.*, 1994, **20**, 257–273.
11. LIANG XU: PhD Thesis, Queen's University, Belfast, 1996.
12. D. W. SUN and R. J. CRAWFORD: *Plastics, Rubber Composites Proc. Appl.*, 1993, **19**, 47–53.
13. X. M. WANG: PhD Thesis, Queen's University, Belfast, 1995.
14. J. L. THRONE: *ANTEC 2002 Plastics: Ann. Tech. Conf.*, 2002, **1**, 67.
15. R. W. LEWIS and P. M. ROBERTS: *Appl. Sci. Res.*, 1987, **44**, 61–92.
16. K. J. BATHE: 'Finite Element Procedures In Engineering Analysis', 1st edn. New Jersey, Prentice-Hall, 1982, 735.
17. D. BURNETT: 'Finite Element Analysis – From Concept to Applications', 1st edn, New Jersey, Addison-Wiesley, 1987, 844.
18. A. J. DALHUIJSEN and A. SEGAL: *Int. J. Num. Method Eng.*, 1986, **23**, 1807–1829.
19. E. J. WRIGHT and R. J. CRAWFORD: 'Computer Simulation of The Rotational Moulding Process of Plastics', ANTEC, 1999, 1441.